Chapter 5

Observing Through the Turbulent Atmosphere

Andreas Quirrenbach

University of California, San Diego
La Jolla, California

5.1 Introduction

Atmospheric turbulence is a major contributor to the difficulty of optical and infrared interferometry from the ground. In fact, many of the key design parameters of an interferometer—site selection, operating wavelength, aperture size, bandwidths of the angle-tracking and fringe-tracking servo loops, coherent integration time, inclusion of adaptive optics—are driven largely by the boundary conditions set by the atmosphere. The sensitivity of interferometers, and the precision of astrometric measurements, depend strongly on the "seeing." It is therefore important to understand how turbulence is generated in the atmosphere, and how its effects on the propagation of light can be quantified. This tutorial is intended to give a brief overview of these topics. Their application to the design and operation of interferometers is discussed in other contributions to this volume.

The organization of the present article is as follows: Section 5.2 introduces the Kolmogorov turbulence model, which gives some physical insight into the generation of turbulence, and which is widely used as a quantitative model to describe the spatial variations of quantities such as density and refractive index in turbulent media. Section 5.3 deals with the propagation of waves through turbulence. In this section, the *Fried parameter* r_0 is defined as a numeric measure of the integrated turbulence strength. Section 5.4 discusses optical image formation and the effects of turbulence on images. It is shown that r_0 is

directly related to the width of seeing-limited images. The parameter τ_0, which measures the coherence time, and the concept of anisoplanatism and the coherence angle θ_0 are introduced. The appendix, Section 5.5, summarizes a few useful facts from Fourier theory.

Due to space constraints, the treatment of the subject matter in this article is necessarily short. More detailed accounts of atmospheric turbulence and its effect on high-angular resolution astronomy can be found in the articles by Roddier (1981 and 1989) and by Fried (1994), as well as in the excellent book by Hardy (1998). The text by Léna, Lebrun, and Mignard (1998) contains a very short summary of atmospheric turbulence in the context of image formation. The book by Born and Wolf (1999) is still the standard resource for general information on the principles of optics.

5.2 The Kolmogorov Turbulence Model

5.2.1 Eddies in the Turbulent Atmosphere

The properties of fluid flows are characterized by the well-known Reynolds number $Re = VL/\nu$, where V is the fluid velocity, L a characteristic length scale, and ν the kinematic viscosity of the fluid. For air, $\nu = 1.5 \cdot 10^{-5}\,\mathrm{m^2\,s^{-1}}$, so that atmospheric flows with winds of a few $\mathrm{m\,s^{-1}}$ and length scales of several meters to kilometers have $Re \gtrsim 10^6$ and are therefore almost always turbulent. The turbulent energy is generated by eddies on a large scale L_0, which spawn a hierarchy of smaller eddies (see also Figure 5.1). Dissipation is not important for the large eddies, but the kinetic energy of the turbulent motion is dissipated in small eddies with a typical size l_0. The characteristic size scales L_0 and l_0 are known as the *outer scale* and the *inner scale* of the turbulence. There is considerable debate over typical values of L_0; it may be a few tens to hundreds of meters in most cases. l_0 is of order a few millimeters.

In the so-called *inertial range* between l_0 and L_0, there is a universal description for the turbulence spectrum, i.e., the strength of the turbulence as a function of the eddy size, or of the spatial frequency κ. This somewhat surprising result is the underlying reason for the importance of this simple turbulence model, which was developed by Kolmogorov, and is generally known as *Kolmogorov turbulence*. In the following section, a simple argument based on dimensional analysis will be used to derive the structure function for the Kolmogorov model.

5.2.2 The Structure Function for Kolmogorov Turbulence

The only two relevant parameters (in addition to l_0 and L_0) that determine the strength and spectrum of Kolmogorov turbulence are the rate of energy generation per unit mass ε, and the kinematic viscosity ν. The units of ε are $\mathrm{J\,s^{-1}\,kg^{-1}} = \mathrm{m^2\,s^{-3}}$, and those of ν are $\mathrm{m^2\,s^{-1}}$. Under the assumption that the turbulence is homogeneous and isotropic, the

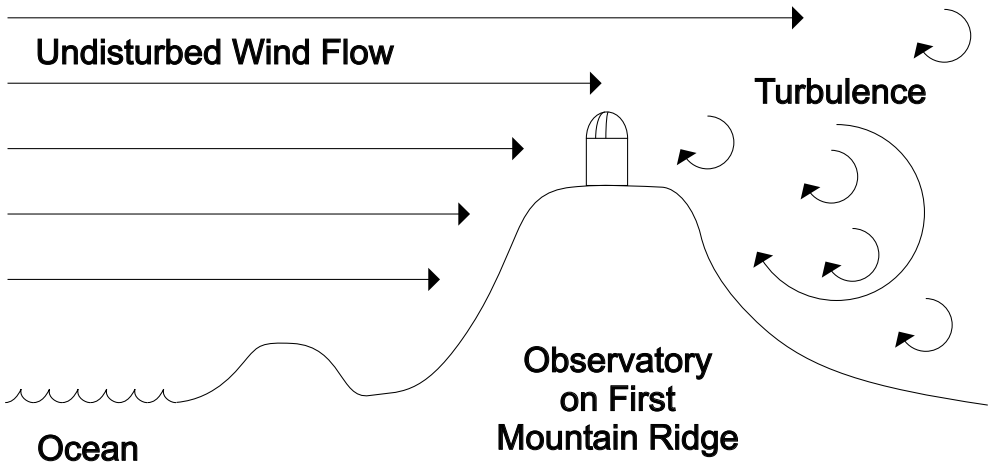

Figure 5.1: Schematic of turbulence generation in the wake of obstacles. Most world-class observatories are located on the first mountain ridge near the coast (or on mountains on islands), with prevailing winds from the ocean.

structure function of the turbulent velocity field, $D_v(R_1, R_2)$, depends only on $|R_1 - R_2|$, and can therefore be written as

$$\begin{aligned} D_v(R_1, R_2) &\equiv \langle |v(R_1) - v(R_2)|^2 \rangle \\ &= \alpha \cdot f\left(|R_1 - R_2| \,/\, \beta\right) \quad , \end{aligned} \tag{5.1}$$

where f is some dimensionless function of a dimensionless argument. It is immediately clear that the dimensions of α are velocity squared, and those of β length. Since α and β depend only on ε and ν, it follows from dimensional analysis that

$$\alpha = \nu^{1/2}\varepsilon^{1/2} \quad \text{and} \quad \beta = \nu^{3/4}\varepsilon^{-1/4} \quad . \tag{5.2}$$

In addition, the structure function must be independent of ν in the inertial range. This is possible only if

$$D_v(R_1, R_2) = \alpha \cdot \left(|R_1 - R_2| \,/\, \beta\right)^{2/3} = C_v^2 \cdot |R_1 - R_2|^{2/3} \quad , \tag{5.3}$$

where C_v^2 is a constant. We have thus derived the important result mentioned above, namely a universal description of the turbulence spectrum. It has only one parameter C_v^2, which describes the turbulence strength.

5.2.3 Structure Function and Power Spectral Density of the Refractive Index

The turbulence, whose velocity field is characterized by Equation 5.3, mixes different layers of air, and therefore carries around "parcels" of air with different temperature. Since these "parcels" are in pressure equilibrium, they have different densities ρ, and therefore different indices of refraction n. It can be shown that the temperature fluctuations also follow Kolmogorov's law with a new parameter C_T^2 of their own:

$$D_T(R_1, R_2) = C_T^2 \cdot |R_1 - R_2|^{2/3} \quad . \tag{5.4}$$

From the ideal gas law, and $N \equiv (n-1) \propto \rho$, it follows that the structure function of the refractive index is

$$D_n(R_1, R_2) = D_N(R_1, R_2) = C_N^2 \cdot |R_1 - R_2|^{2/3} \quad , \tag{5.5}$$

with

$$C_N = (7.8 \cdot 10^{-5} P[\text{mbar}]/T^2[\text{K}]) \cdot C_T \quad . \tag{5.6}$$

We note that Equation 5.5 contains a complete description of the statistical properties of the refractive index fluctuations, on length scales between l_0 and L_0. It is possible to calculate related quantities such as the power spectral density Φ from the structure function D. Using the relation between the structure function and the covariance (Equation 5.51), and the Wiener–Khinchin Theorem (Equation 5.49), we obtain

$$C_N^2 \cdot R^{2/3} = D_N(R) = 2 \int_{-\infty}^{\infty} d\kappa \, (1 - \exp(2\pi i \kappa R)) \, \Phi(\kappa) \quad . \tag{5.7}$$

Calculating $\Phi(\kappa)$ from this relation is a slightly non-trivial task*; the result is

$$\Phi(\kappa) = \frac{\Gamma(\frac{5}{3}) \sin \frac{\pi}{3}}{(2\pi)^{5/3}} \, C_N^2 \kappa^{-5/3} = 0.0365 \, C_N^2 \kappa^{-5/3} \quad . \tag{5.8}$$

We have thus obtained the important result that the power spectrum of Kolmogorov turbulence follows a $\kappa^{-5/3}$ law in the inertial range.†

5.3 Wave Propagation Through Turbulence

5.3.1 The Effects of Turbulent Layers

We now look at the propagation of a wavefront $\psi(x) = \exp i\phi(x)$ through a turbulent layer of thickness δh at height h. The phase shift produced by refractive index fluctuations is

$$\phi(x) = k \int_{h}^{h+\delta h} dz \, n(x, z) \quad , \tag{5.9}$$

where $k = 2\pi/\lambda$. For layers that are much thicker than the individual turbulence cells, many independent variables contribute to the phase shift, which therefore has Gaussian statistics according to the Central Limit Theorem.

The task at hand is now using the statistical properties of the refractive index fluctuations, which were calculated in Section 5.2.3, to derive the statistical properties of the wavefront.

---

*See Tatarski (1961). Note that his definition of the power spectral density has an additional factor $\frac{1}{2\pi}$, and that his ω corresponds to $2\pi\kappa$.

†Note: We have defined $R = |R_1 - R_2|$ and κ as one-dimensional variables, and consequently used a one-dimensional Fourier transform in Equation 5.7. Sometimes three-dimensional quantities $\vec{R}$ and $\vec{\kappa}$ are used instead. Then a three-dimensional Fourier transform with volume element $4\pi \, |\vec{\kappa}|^2 \, d\,|\vec{\kappa}|$ has to be used in Equation 5.7, and the result is a power spectrum $\Phi(|\vec{\kappa}|) \propto |\vec{\kappa}|^{-11/3}$.

We first express the coherence function $B_h(r)$ of the wavefront after passing through the layer at height h in terms of the phase structure function:

$$\begin{aligned} B_h(r) &\equiv \langle \psi(x)\psi^*(x+r)\rangle \\ &= \langle \exp i\,[\phi(x)-\phi(x+r)]\rangle \\ &= \exp\left(-\tfrac{1}{2}\langle|\phi(x)-\phi(x+r)|^2\rangle\right) \\ &= \exp\left(-\tfrac{1}{2}D_\phi(r)\right) \quad . \end{aligned} \tag{5.10}$$

Here we have used the fact that $[\phi(x)-\phi(x+r)]$ has Gaussian statistics with zero mean, and the relation

$$\langle \exp(\alpha\chi)\rangle = \exp\left(\tfrac{1}{2}\alpha^2\langle\chi^2\rangle\right) \tag{5.11}$$

for Gaussian variables χ with zero mean, which can easily be verified by carrying out the integral over the distribution function.

5.3.2 Calculation of the Phase Structure Function

The next step is the computation of $D_\phi(r)$. We start with the covariance $B_\phi(r)$, which is by definition:

$$\begin{aligned} B_\phi(r) &\equiv \langle \phi(x)\phi(x+r)\rangle \\ &= k^2\int_h^{h+\delta h}\int_h^{h+\delta h} dz'\,dz''\,\langle n(x,z')n(x+r,z'')\rangle \\ &= k^2\int_h^{h+\delta h} dz' \int_{h-z'}^{h+\delta h-z'} dz\,B_N(r,z) \quad . \end{aligned} \tag{5.12}$$

Here we have introduced the new variable $z = z'' - z'$, and the covariance $B_N(r,z)$ of the refractive index variations. For δh much larger than the correlation scale of the fluctuations, the integration can be extended from $-\infty$ to ∞, and we obtain

$$B_\phi(r) = k^2\delta h\int_{-\infty}^{\infty} dz\,B_N(r,z) \quad . \tag{5.13}$$

Now we can use Equation 5.51 again, first for $D_\phi(r)$, then for $D_N(r,z)$ and $D_N(0,z)$, and get:

$$\begin{aligned} D_\phi(r) &= 2[B_\phi(0)-B_\phi(r)] \\ &= 2k^2\delta h\int_{-\infty}^{\infty} dz\,[B_N(0,z)-B_N(r,z)] \\ &= 2k^2\delta h\int_{-\infty}^{\infty} dz\,\Big[(B_N(0,0)-B_N(r,z))-(B_N(0,0)-B_N(0,z))\Big] \\ &= k^2\delta h\int_{-\infty}^{\infty} dz\,[D_N(r,z)-D_N(0,z)] \quad . \end{aligned} \tag{5.14}$$

Inserting from Equation 5.5 gives

$$\begin{aligned} D_\phi(r) &= k^2 \delta h\, C_N^2 \int_{-\infty}^{\infty} dz \, \left[\left(r^2 + z^2\right)^{1/3} - |z|^{2/3} \right] \\ &= \frac{2\Gamma(\frac{1}{2})\Gamma(\frac{1}{6})}{5\Gamma(\frac{2}{3})}\, k^2 \delta h\, C_N^2\, r^{5/3} \\ &= 2.914\, k^2 \delta h\, C_N^2\, r^{5/3} \quad . \end{aligned} \tag{5.15}$$

This is the desired expression for the structure function of phase fluctuations due to Kolmogorov turbulence in a layer of thickness δh.

5.3.3 Phase-Coherence Function and Fried Parameter

We are now in a position to put everything together. Inserting Equation 5.15 into Equation 5.10, we get

$$B_h(r) = \exp\left[-\tfrac{1}{2} \left(2.914\, k^2 C_N^2\, \delta h\, r^{5/3}\right) \right] \quad . \tag{5.16}$$

Integration over the whole atmosphere, and taking into account the zenith angle z, gives:

$$B(r) = \exp\left[-\tfrac{1}{2} \left(2.914\, k^2 (\sec z) r^{5/3} \int dh\, C_N^2(h) \right) \right] \quad . \tag{5.17}$$

We now define the *Fried parameter* r_0 by

$$r_0 \equiv \left[0.423\, k^2 (\sec z) \int dh\, C_N^2(h) \right]^{-3/5} \tag{5.18}$$

and can write

$$B(r) = \exp\left[-3.44 \left(\frac{r}{r_0} \right)^{5/3} \right] \quad , \quad D(r) = 6.88 \left(\frac{r}{r_0} \right)^{5/3} \quad . \tag{5.19}$$

We have thus derived fairly simple expressions for the phase-coherence function and the phase structure function. They depend only on the Fried parameter r_0, which in turn is a function of turbulence strength, zenith angle, and wavelength. The significance of the Fried parameter will be discussed further in Section 5.4.3.

5.4 The Effect of Turbulence on Images

5.4.1 Optical Image Formation

The complex amplitude A of a wave ψ diffracted at an aperture P with area Π is given by Huygens' principle, which states that each point in the aperture can be considered as the center of an emerging spherical wave. In the far field (i.e., in the case of Fraunhofer

diffraction), the spherical waves are equivalent to plane waves, and we can write down the expression for the amplitude:

$$A(\alpha) = \frac{1}{\sqrt{\Pi}} \int dx\, \psi(x) P(x) \exp(-2\pi i \alpha x/\lambda) \quad . \tag{5.20}$$

Here we describe the aperture P by a complex function $P(x)$; in the simple case of a fully transmissive aperture without aberrations $P(x) \equiv 1$ inside the aperture, and $P(x) \equiv 0$ outside. Introducing the new variable $u \equiv x/\lambda$ we can write

$$A(\alpha) = \frac{1}{\sqrt{\Pi}} FT[\psi(u)P(u)] \quad . \tag{5.21}$$

The normalization in equations 5.20 and 5.21 has been chosen such that the illumination in the focal plane is given by the square of the wave amplitude:

$$S(\alpha) = |A(\alpha)|^2 = \frac{1}{\Pi} \left| FT[\psi(u)P(u)] \right|^2 \quad . \tag{5.22}$$

Applying the Wiener–Khinchin Theorem (Equation 5.49) to this equation we get

$$S(f) = \frac{1}{\Pi} \int du\, \psi(u)\psi^*(u+f) P(u) P^*(u+f) \quad . \tag{5.23}$$

This equation can be used to describe the spatial frequency content $S(f)$ of images taken through the turbulent atmosphere if ψ is identified with the wavefront after passing through the turbulence. Taking long exposures (in practice this means exposures of at least a few seconds) means averaging over different realizations of the atmosphere:

$$\begin{aligned} \langle S(f) \rangle &= \frac{1}{\Pi} \int du\, \langle \psi(u)\psi^*(u+f) \rangle P(u) P^*(u+f) \\ &= B_\psi(f) \cdot T(f) \quad . \end{aligned} \tag{5.24}$$

Here we have introduced the *telescope transfer function*

$$T(f) = \frac{1}{\Pi} \int du\, P(u) P^*(u+f) \quad . \tag{5.25}$$

Equation 5.24 contains the important result that for long exposures the optical transfer function is the product of the telescope transfer function and the atmospheric transfer function, which is equal to the phase-coherence function $B_\psi(f)$.

5.4.2 Diffraction-Limited Images and Seeing-Limited Images

The resolving power R of an optical system can very generally be defined by the integral over the optical transfer function. For the atmosphere/telescope system we get

$$R \equiv \int df\, S(f) = \int df\, B(f) T(f) \quad . \tag{5.26}$$

In the absence of turbulence, $B(f) \equiv 1$, and we obtain the *diffraction-limited* resolving power of a telescope with diameter D:

$$\begin{aligned} R_{\rm tel} &= \int df\, T(f) = \frac{1}{\Pi}\int\int du df\, P(u)P^*(u+f) \\ &= \frac{1}{\Pi}\left|\int du\, P(u)\right|^2 = \frac{\pi}{4}\left(\frac{D}{\lambda}\right)^2 \quad . \end{aligned} \tag{5.27}$$

The last equality assumes a circular aperture and shows the relation of R to the familiar Rayleigh criterion $1.22\cdot\lambda/D$. The advantage of using R over the Rayleigh criterion is that R is a well-defined quantity for arbitrary aperture shapes and in the presence of aberrations.

For strong turbulence and rather large telescope diameters, $T = 1$ in the region where B is non-zero, and we get the *seeing-limited* resolving power:

$$\begin{aligned} R_{\rm atm} &= \int df\, B(f) = \int df \exp\left[-\left(3.44\left(\tfrac{\lambda f}{r_0}\right)^{5/3}\right)\right] \\ &= \frac{6\pi}{5}\Gamma(\tfrac{6}{5})\left(3.44\left(\tfrac{\lambda}{r_0}\right)^{5/3}\right)^{-6/5} = \frac{\pi}{4}\left(\frac{r_0}{\lambda}\right)^2 \quad . \end{aligned} \tag{5.28}$$

Here we have used Equation 5.19 with $r = \lambda f$ for the phase-coherence function $B(f)$.

5.4.3 The Significance of the Fried Parameter r_0

A comparison of Equations 5.27 and 5.28 elucidates the significance of the Fried parameter, and reveals the reason for the peculiar choice of the numerical parameter 0.423 in Equation 5.18: *The resolution of seeing-limited images obtained through an atmosphere with turbulence characterized by a Fried parameter r_0 is the same as the resolution of diffraction-limited images taken with a telescope of diameter r_0.* Observations with telescopes much larger than r_0 are seeing-limited, whereas observations with telescopes smaller than r_0 are essentially diffraction-limited. It can also be shown that the mean-square phase variation over an aperture of diameter r_0 is about $1\,\mathrm{rad}^2$ (more precisely, $\sigma_\phi^2 = 1.03\,\mathrm{rad}^2$). These results are captured in the extremely simplified picture that describes the atmospheric turbulence by r_0-sized "patches" of constant phase, and random phases between the individual patches. While this picture can be useful for some rough estimates, one should keep in mind that Kolmogorov turbulence has a continuous spectrum ranging from l_0 to L_0.

The scaling of r_0 with wavelength and zenith angle implied by Equation 5.18 has far-reaching practical consequences. Since

$$r_0 \propto \lambda^{6/5} \quad , \tag{5.29}$$

it is much easier to achieve diffraction-limited performance at longer wavelengths. For example, the number of degrees of freedom (the number of actuators on the deformable mirror and the number of subapertures in the wavefront sensor) in an adaptive optics system must be of order $(D/r_0)^2 \propto \lambda^{-12/5}$. An interferometer works well only if the wavefronts from the individual telescopes are coherent (i.e., have phase variances not larger than about

$1\,\mathrm{rad}^2$); therefore the maximum useful aperture area of an interferometer is $\propto \lambda^{12/5}$ (unless the wavefronts are corrected with adaptive optics). Equation 5.29 implies that the width of seeing-limited images, $\theta \simeq 1.2 \cdot \lambda/r_0 \propto \lambda^{-1/5}$, varies only slowly with λ; it is somewhat better at longer wavelengths. In addition, we see from Equation 5.18 that $r_0 \propto (\sec z)^{-3/5}$; the effects of seeing increase with air mass.

From this discussion it should be clear that the magnitude of r_0—given by the integral over C_N^2—is a crucial parameter for high-resolution observations. At good sites, such as Mauna Kea, r_0 is of order 20 cm at 500 nm, which corresponds to an image FWHM of $0.''6$. The scaling of r_0 with λ (Equation 5.29) implies that in the mid-infrared ($\lambda \gtrsim 10\,\mu$m) even the 10 m Keck Telescopes are nearly diffraction-limited, whereas a 1.8-m telescope has $D/r_0 \sim 2$ at $\lambda = 2\,\mu$m and $D/r_0 \sim 5$ at $\lambda = 800$ nm. It should be noted that at any given site r_0 varies dramatically from night to night; it may be a factor of 2 better than the median or a factor of 5 worse. In addition, the seeing fluctuates on all time scales down to minutes and seconds; this has to be taken into account in calibration procedures.

5.4.4 Strehl Ratio

The quality of an imaging system, or of the wavefront after propagation through turbulence, is often measured by the *Strehl ratio* S, defined as the peak intensity in the image of a point source divided by the peak intensity in a diffraction-limited image taken through the same aperture. For a circular aperture with an aberration function $\psi(\rho, \theta)$, which describes the wavefront distortion (in μm or nm) as a function of the spherical coordinates (ρ, θ), the Strehl ratio is given by:

$$S = \frac{1}{\pi^2} \left| \int_0^1 \int_0^{2\pi} \rho \, d\rho \, d\theta \, e^{ik\psi(\rho,\theta)} \right|^2 \quad . \tag{5.30}$$

From this equation it is immediately clear that $0 \leq S \leq 1$, that $S = 1$ for $\psi = \text{const.}$, that $S \ll 1$ for strongly varying ψ, and that for any given (varying) ψ the Strehl ratio tends to be larger for longer wavelengths (smaller k). In the case of atmospheric turbulence, only the statistical properties of ψ are known. If the rms wavefront error $\sigma_\phi \equiv k\,\sigma_\psi$ is smaller than about 2 rad, S can be approximated by the so-called *extended Marechal approximation*:

$$S = e^{-\sigma_\phi^2} \quad . \tag{5.31}$$

We have seen above (Equation 5.19 and Section 5.4.3) that

$$\sigma_\phi^2 = 1.03 \left(\frac{D}{r_0} \right)^{5/3} \quad . \tag{5.32}$$

Equations 5.31 and 5.32 show that the Strehl ratio for a telescope with diameter $D = r_0$ is $S = 0.36$; for $D \gtrsim r_0$ the Strehl ratio decreases precipitously with telescope diameter. (Equivalently S decreases sharply with decreasing wavelength, since $r_0 \propto \lambda^{6/5}$.)

If $S \gtrsim 0.1$ in an imaging application, deconvolution algorithms can usually be applied to obtain diffraction-limited images, but the dynamic range and signal-to-noise ratio are worse

than for $S \sim 1$. For example, because of spherical aberration, the Hubble Space Telescope has $S \simeq 0.1$ without corrective optics. Before the installation of COSTAR and WFPC2 in the first servicing mission, the imaging performance of HST was severely affected by the flawed optics, although diffraction-limited images could be obtained with image restoration software. In an interferometer, the maximum fringe contrast is roughly proportional to the Strehl ratio if no corrective measures (adaptive optics or mode filtering with pinholes or single-mode fibers) are taken.

5.4.5 Taylor Hypothesis and τ_0

So far we have discussed the spatial structure of atmospheric turbulence and its effects on image formation. Now we turn to the question of temporal changes of the turbulence pattern. The time scale for these changes is usually much longer than the time it takes the wind to blow the turbulence past the telescope aperture. According to the *Taylor hypothesis of frozen turbulence*, the variations of the turbulence caused by a single layer can therefore be modeled by a "frozen" pattern that is transported across the aperture by the wind in that layer. If multiple layers contribute to the total turbulence, the time evolution is more complicated, but the temporal behavior of the turbulence can still be characterized by a time constant

$$\tau_0 \equiv r_0/v \quad , \tag{5.33}$$

where v is the wind speed in the dominant layer. With typical wind speeds of order 20 m/s, $\tau_0 \simeq 10$ ms for $r_0 = 20$ cm. The wavelength scaling of τ_0 is obviously the same as that of r_0, i.e., $\tau_0 \propto \lambda^{6/5}$.

Observations with exposure time $t \gg \tau_0$ average over the atmospheric random process; these are the *long exposures* for which Equations 5.24 and 5.28 are applicable. In contrast, *short exposures* with $t \ll \tau_0$ produce images through a single instantaneous realization of the atmosphere; these *speckle images* contain information at high spatial frequencies up to the diffraction limit, which can be extracted from series of such images with computer processing (e.g., bispectrum analysis). The parameter τ_0 is also of great importance for the design of adaptive optics systems and interferometers. All control loops that have to reject atmospheric fluctuations—AO control loops, angle trackers, fringe trackers—must have bandwidths larger than $1/\tau_0$. Together r_0 and τ_0 set fundamental limits to the sensitivity of these wavefront control loops: a certain number of photons must arrive per r_0-sized patch during the time τ_0 for the wavefront sensor (or fringe sensor) to work. This implies that the sensitivity scales with $r_0^2 \cdot \tau_0 \propto \lambda^{18/5}$ (for equal photon flux per bandpass).

5.4.6 Anisoplanatism

The light from two stars separated by an angle θ passes through different patches of the atmosphere and therefore experiences different phase variations. This *angular anisoplanatism* limits the field corrected by adaptive optics systems and causes phase decorrelation for off-axis objects in interferometers. To calculate the effect of anisoplanatism, we trace

back the rays to two stars separated by an angle θ from the telescope pupil. They coincide at the pupil, and their separation $r(d)$ at a distance d is $\theta \cdot d$. At zenith angle z, the distance is related to the height h in the atmosphere by $d = h \sec z$. To calculate the phase variance between the two rays, we insert this relation in

$$D_\phi(r) = 2.914\, k^2 \sec z\, \delta h\, C_N^2\, r^{5/3} \tag{5.34}$$

(see Equation 5.15) and obtain

$$\begin{aligned} \langle \sigma_\theta^2 \rangle &= 2.914\, k^2 (\sec z) \int dh\, C_N^2(h)\, (\theta h \sec z)^{5/3} \\ &= 2.914\, k^2 (\sec z)^{8/3} \theta^{5/3} \int dh\, C_N^2(h) h^{5/3} \\ &= \left(\frac{\theta}{\theta_0} \right)^{5/3} \quad , \end{aligned} \tag{5.35}$$

where we have introduced the *isoplanatic angle* θ_0, for which the variance of the relative phase is $1\,\mathrm{rad}^2$:

$$\theta_0 \equiv \left[2.914\, k^2 (\sec z)^{8/3} \int dh\, C_N^2(h) h^{5/3} \right]^{-3/5} \quad . \tag{5.36}$$

By comparing the definitions for the Fried parameter r_0 and for θ_0, (Equations 5.18 and 5.36), we see that

$$\theta_0 = 0.314\, (\cos z)\, \frac{r_0}{H} \quad , \tag{5.37}$$

where

$$H \equiv \left(\frac{\int dh\, C_N^2(h) h^{5/3}}{\int dh\, C_N^2(h)} \right)^{3/5} \tag{5.38}$$

is the *mean effective turbulence height*. Equations 5.36 and 5.37 show that the isoplanatic angle is affected mostly by high-altitude turbulence; the anisoplanatism associated with ground layers and dome seeing is very weak. Moreover, we see that θ_0 scales with $\lambda^{6/5}$, but it depends more strongly on zenith angle than r_0. For $r_0 = 20\,\mathrm{cm}$ and an effective turbulence height of $7\,\mathrm{km}$, Equation 5.37 gives $\theta_0 = 1.8\,\mathrm{arcsec}$. For two stars separated by more than θ_0 the short-exposure point-spread functions (or point-spread functions generated by adaptive optics) are different.[‡] In contrast the long-exposure point-spread functions, which represent averages over many realizations of the atmospheric turbulence, are nearly identical even over angles much larger than θ_0.

[‡]It should be pointed out that these calculations of anisoplanatism give somewhat too pessimistic results. The reason is that a large fraction of the phase variance between the two rays considered is a piston term which doesn't lead to image motion or blurring. (Note, however, that the piston term has to be taken into account in interferometry.) Moreover, anisoplanatism is less severe for low spatial frequencies, which most adaptive optics systems correct much better than high spatial frequencies. The degradation of the Strehl ratio with off-axis angle is therefore not quite as bad as suggested by inserting Equation 5.35 in Equation 5.31.

5.4.7 Scintillation

The geometric optics approximation of light propagation that was used in Section 5.3 is only valid for propagation pathlengths shorter than the *Fresnel propagation length* $d_F \equiv r_0^2/\lambda$. (In other words, the Fresnel scale $r_F \equiv \sqrt{\lambda L}$, where L is the distance to the dominant layer of turbulence, must be smaller than the Fried scale r_0.) For $r_0 = 20\,\mathrm{cm}$ and $\lambda = 500\,\mathrm{nm}$, $d_F = 80\,\mathrm{km}$, and the geometric approximation is a good first-order approach at good sites for visible and infrared wavelengths (since $d_F \propto \lambda^{7/5}$ for Kolmogorov turbulence). However, if the propagation length is comparable to d_F or longer, the rays diffracted at the turbulence cells interfere with each other, which causes intensity fluctuations in addition to the phase variations. This phenomenon is called *scintillation*; it is an important error source in high-precision photometry unless the exposure times are very long. Since scintillation is an interference phenomenon, it is highly chromatic. This effect can be easily observed with the naked eye: bright stars close to the horizon twinkle strongly and change color on time scales of seconds.

Although scintillation is weak for most applications of adaptive optics and interferometry, it has to be taken into account under some circumstances. For example, high-performance adaptive optics systems designed for the direct detection of extrasolar planets have to correct the wavefront errors so well that intensity fluctuations become important. In interferometers that use fringe detection schemes based on temporal pathlength modulation and synchronous photon detection, scintillation noise has to be considered when very small fringe amplitudes are to be measured.

The effects of scintillation can be quantified by determining the relative intensity fluctuations $\delta I/I$; for small amplitudes $\delta I/I = \delta \ln I$. A calculation similar to the one in Section 5.3 gives the variance of the log intensity fluctuations:

$$\sigma^2_{\ln I} = 2.24\, k^{7/6} (\sec z)^{11/6} \int dh\, C_N^2(h) h^{5/6} \quad . \tag{5.39}$$

This expression is valid only for small apertures with diameter $D \ll r_F$. For larger apertures, scintillation is reduced by averaging over multiple independent subapertures. This changes not only the amplitude of the intensity fluctuations, but also the functional dependence on zenith angle, wavelength, and turbulence height. The expression

$$\sigma^2_{\ln I} \propto D^{-7/3} (\sec z)^3 \int dh\, C_N^2(h) h^2 \quad , \tag{5.40}$$

which is valid for $D \gg r_F$ and $z \lesssim 60°$, shows the expected strong decrease of the scintillation amplitude with aperture size; note that it is independent of the observing wavelength. For larger zenith angles the assumption $\delta \ln I \ll 1$ is no longer valid, the fluctuations increase less strongly with $\sec z$ than predicted by Equation 5.40, and eventually saturate.

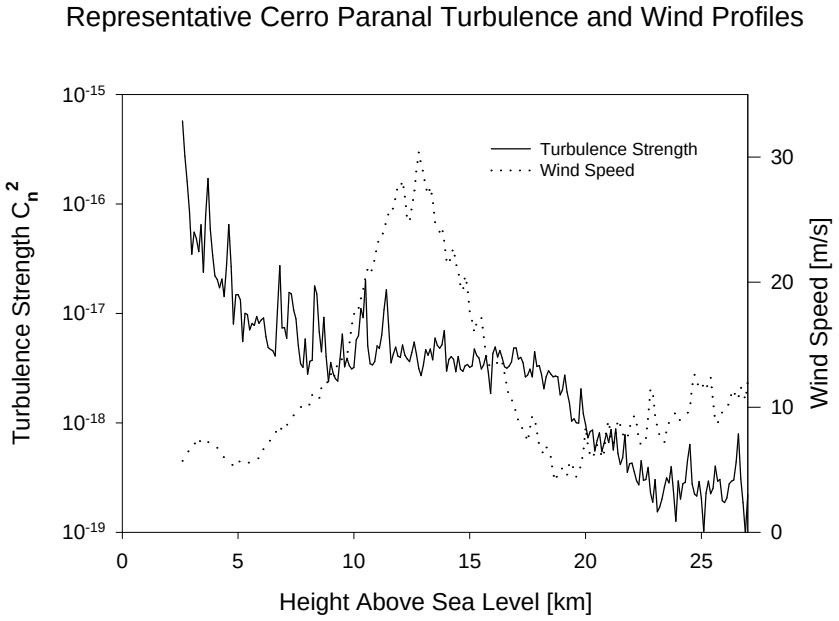

Figure 5.2: Turbulence and wind profiles measured on Cerro Paranal, Chile. The turbulence is strongest close to the ground (2635 m above sea level). The wind speed is highest at an altitude of ~ 10 to 15 km. Wind shear often leads to additional layers of strong turbulence at high altitude (only weakly present in this data set).

5.4.8 Turbulence and Wind Profiles

We have seen in the preceding sections that the most important statistical properties of seeing can be characterized by a few numbers: the Fried parameter r_0, the coherence time τ_0, the isoplanatic angle θ_0, and the scintillation index $\sigma_{\ln I}$. For the design and performance evaluation of high-angular-resolution instruments it is of great importance to have reliable statistical information on these parameters. Therefore extensive seeing monitoring campaigns are normally conducted before decisions are made about the site selection for large telescopes and interferometers, or about the construction of expensive adaptive optics systems. Having access to the output of a continuously running seeing monitor which gives the instantaneous value of r_0 (and ideally also of the other seeing parameters) is also very convenient for debugging and for optimizing the performance of high-resolution instruments.

From Equations 5.18, 5.33, 5.35, and 5.39 it is obvious that all seeing parameters can easily be calculated from moments

$$\mu_m \equiv \int dh\, C_N^2(h) h^m \tag{5.41}$$

of the turbulence profile $C_N^2(h)$; and (in the case of τ_0) from moments

$$v_m \equiv \int dh\, C_N^2(h) v^m(h) \tag{5.42}$$

of the wind profile $v(h)$. More complicated analyses such as performance estimates of adaptive optics systems with laser guide stars and of multi-conjugate AO systems also rely on knowledge of $C_N^2(h)$ and $v(h)$. In-situ measurements of these profiles with balloon flights and remote measurements with SCIDAR[§] or related methods are therefore needed to fully characterize the atmospheric turbulence. Figure 5.2 shows profiles measured on Cerro Paranal, the site of the European Southern Observatory's Very Large Telescope observatory. The decrease of C_N^2 with height is typical for most sites; frequently wind shear at altitudes near 10 km creates additional layers of enhanced turbulence. The highest wind speeds normally occur at heights between 9 and 12 km. Extensive sets of observed turbulence and wind profiles, combined with the analytic methods sketched in this article and numerical simulations, form a firm basis for the evaluation of astronomical sites, and for the design of interferometers and adaptive optics systems.

5.5 Appendix: Some Useful Facts from Fourier Theory

For reference, this appendix lists a few useful results from Fourier theory without proofs. In the notation adopted, $g \Longleftrightarrow G$ means "G is the Fourier transform of g," and it is understood that $g \Longleftrightarrow G$ and $h \Longleftrightarrow H$. H^* is the complex conjugate of H. Introductions into Fourier theory and more details can be found in many textbooks, for example the one by Bracewell (1999).

The *convolution* $g * h$ and *correlation* $\mathrm{Corr}(g, h)$ of two functions g and h are defined by:

$$g * h \equiv \int_{-\infty}^{\infty} d\tau \, g(t - \tau) h(\tau) \tag{5.43}$$

and

$$\mathrm{Corr}(g, h) \equiv \int_{-\infty}^{\infty} d\tau \, g(t + \tau) h(\tau) \quad . \tag{5.44}$$

A special case of the latter is the correlation of a function with itself, the *covariance*:

$$B_g \equiv \mathrm{Corr}(g, g) \quad . \tag{5.45}$$

For complex functions, the *coherence function* is defined by:

$$B_g \equiv \mathrm{Corr}(g, g^*) \quad . \tag{5.46}$$

The customary use of the same symbol B for covariance and coherence function is somewhat unfortunate, but should not be too confusing.

The famous *Convolution Theorem* and *Correlation Theorem* are:

$$g * h \Longleftrightarrow G(f) H(f) \tag{5.47}$$

[§]The SCIDAR technique is based on auto-correlating pupil images of double stars.

and

$$\mathrm{Corr}(g,h) \Longleftrightarrow G(f)H^*(f) \quad . \tag{5.48}$$

The special case of the Correlation Theorem for the covariance is the *Wiener–Khinchin Theorem*:

$$B_g = \mathrm{Corr}(g,g) \Longleftrightarrow |G(f)|^2 \quad . \tag{5.49}$$

The *structure function* D_g of a function g is defined by:

$$D_g(t_1,t_2) \equiv \langle |g(t_1) - g(t_2)|^2 \rangle \quad . \tag{5.50}$$

If g describes a homogeneous and isotropic random process, D_g depends only on $t = |t_1 - t_2|$. By expanding the square in Equation 5.50, we see that in this case

$$D_g(t) = 2\left(B_g(0) - B_g(t)\right) \quad . \tag{5.51}$$

Finally, *Parseval's Theorem* states that the total power in a time series is the same as the total power in the corresponding spectrum:

$$\text{Total Power} \equiv \int_{-\infty}^{\infty} dt\, |g(t)|^2 = \int_{-\infty}^{\infty} df\, |G(f)|^2 \quad . \tag{5.52}$$

References

M. Born and E. Wolf, *Principles of Optics*, 7 edn. (Cambridge, UK: Cambridge University Press, 1999).

R.N. Bracewell, *The Fourier Transform and its Applications*, 3 edn. (New York: McGraw-Hill, 1999).

D.L. Fried, "Atmospheric Turbulence Optical Effects: Understanding the Adaptive-Optics Implications," in *Adaptive Optics for Astronomy*, D.M. Alloin and J.-M. Mariotti eds., NATO ASI Series **423** (Dordrecht, Netherlands: Kluwer Academic, 1994), 25–57.

J.W. Hardy, *Adaptive Optics for Astronomical Telescopes* (Oxford, UK: Oxford University Press, 1998).

P. Léna, F. Lebrun, and F. Mignard, *Observational Astrophysics*, 2 edn. (Berlin, Germany: Springer-Verlag, 1998).

F. Roddier, "The effects of atmospheric turbulence in optical astronomy," Prog. Opt. **19**, 281–376 (1981).

F. Roddier, "Optical Propagation and Image Formation through the Turbulent Atmosphere," in *Diffraction-Limited Imaging with Very Large Telescopes*, D.M. Alloin and J.-M. Mariotti eds., NATO ASI Series Vol. **274** (Dordrecht, Netherlands: Kluwer Academic, 1989), 33–52.

V.I. Tatarski, *Wave Propagation in a Turbulent Medium* (New York: McGraw-Hill, 1961).